



HHS Public Access

Author manuscript

Cell Rep. Author manuscript; available in PMC 2016 August 31.

Published in final edited form as:

Cell Rep. 2016 August 23; 16(8): 2169–2177. doi:10.1016/j.celrep.2016.07.042.

A Link Between Integral Membrane Protein Expression and Simulated Integration Efficiency

Stephen S. Marshall[#], Michiel J. M. Niesen[#], Axel Müller, Katrin Tiemann, Shyam M. Saladi, Rachel P. Galimidi, Bin Zhang, William M. Clemons Jr^{1,2}, and Thomas F. Miller III¹

Department of Chemistry and Chemical Engineering, California Institute of Technology, Pasadena, CA 91125, USA

[#] These authors contributed equally to this work.

Abstract

Integral membrane proteins (IMP) control the flow of information and nutrients across cell membranes, yet IMP mechanistic studies are hindered by difficulties in expression. We investigate this issue by addressing the connection between IMP sequence and observed expression levels. For homologs of the IMP TatC, observed expression levels widely vary and are affected by small changes in protein sequence. The effect of sequence changes on experimentally observed expression levels strongly correlates with the simulated integration efficiency obtained from coarse-grained modeling, which is directly confirmed using an *in vivo* assay. Furthermore, mutations that improve the simulated integration efficiency likewise increase the experimentally observed expression levels. Demonstration of these trends in both *Escherichia coli* and *Mycobacterium smegmatis* suggests that the results are general to other expression systems. This work suggests that IMP integration is a determinant for successful expression, raising the possibility of controlling IMP expression via rational design.

Introduction

The central role of IMPs in many biological functions motivates structural and biophysical studies that require large amounts of purified protein, often at considerable costs in terms of both materials and labor. A key obstacle is that only a small percentage of IMPs can be overexpressed (*i.e.* heterologously produced at levels conducive to further study) (Lewinson et al., 2008). While extensive efforts have shown promising results for individual IMPs, including those focusing on expression conditions, host modification, and directed evolution (Reviewed in (Schlegel et al., 2010, Wagner et al., 2006, Scott et al., 2013)), none of these

¹Correspondence: tfm@caltech.edu (TFM).

²Lead Contact: clemons@caltech.edu (WMC)

Publisher's Disclaimer: This is a PDF file of an unedited manuscript that has been accepted for publication. As a service to our customers we are providing this early version of the manuscript. The manuscript will undergo copyediting, typesetting, and review of the resulting proof before it is published in its final citable form. Please note that during the production process errors may be discovered which could affect the content, and all legal disclaimers that apply to the journal pertain.

Author contributions

S.S.M., M.J.M.N., A.M., W.M.C. and T.F.M. designed research; S.S.M. and M.J.M.N. performed research; S.S.M., M.J.M.N., A.M., K.T., S.M.S., R.P.G., and B.Z. contributed new reagents/analytic tools; S.S.M., M.J.M.N., A.M., W.M.C. and T.F.M. analyzed data; and S.S.M., M.J.M.N., W.M.C. and T.F.M. wrote the paper.

has proven broadly applicable, even among homologs of a given IMP. In general, the determinants for IMP expression are poorly understood, leading to the prevailing opinion that problems in membrane protein expression must be addressed on a case-by-case basis.

Closely related IMP homologs can vary dramatically in the amount of protein available after expression (Lewinson et al., 2008), which raises a fundamental question: What differentiates the expression of IMP homologs? The hypothesis raised here is that the efficiency with which an IMP is integrated into the membrane is a key determinant in the degree of observed IMP expression.

A fundamental step in the biosynthesis of most IMPs involves their targeting to and integration into the membrane via the Sec protein translocation channel (Rapoport, 2007). Integration of IMP transmembrane domains (TMDs) into the membrane is facilitated primarily through interaction between the nascent chain and SecY, which forms the core of the protein translocation complex, or translocon. Following the co-translational or post-translational insertion of nascent-protein sequences into the translocon channel, hydrophobic segments pass through the lateral gate of SecY into the membrane to form TMDs. Factors such as TMD hydrophobicity (Harley et al., 1998, Hessa et al., 2005) and loop charge (von Heijne, 1986, Goder and Spiess, 2003) have been shown to affect the efficiency of TMD integration and topogenesis. For example, TMD hydrophobicity is directly related to the probability with which TMDs partition into the lipid bilayer, while positively charged residues in the loop alter TMD orientation by preferentially occupying the cytosol (Goder and Spiess, 2003, Hessa et al., 2005, von Heijne, 1986).

In this study, we investigate the connection between observed IMP expression levels and Sec-facilitated IMP integration efficiency (*i.e.*, the probability of membrane integration with the correct multi-spanning topology). Systematic investigation of chimeras within an IMP family leads to the identification of sequence elements that modulate expression levels. *In silico* modeling of IMP integration at the Sec translocation channel finds that the sequence modifications that increase the calculated IMP integration efficiency correlates with *in vivo* overexpression improvements, suggesting that IMP integration efficiency is a determinant for successful expression. The result is found to be general across distinct expression systems (*E. coli* and *M. smegmatis*). Furthermore, an *in vivo* assay based on antibiotic resistance in *E. coli* experimentally confirmed the model that the integration efficiency of an individual TMD correlates with the observed IMP expression levels. The strong link between the effect of sequence modifications on simulated integration efficiency and experimentally measured expression levels offers future promise for the rational design of IMP systems with increased expression levels.

Results

As a detailed case study, the TatC IMP family is employed for all experimental and computational results reported here. A component of the bacterial twin-arginine translocation pathway, TatC plays a key role in the transport of folded proteins across the cytoplasmic membrane (Bogsch et al., 1998). The employment of TatC is well-suited for the current study as it is reasonably sized (only six TMDs (Figure 1A)), non-essential, and

found broadly throughout bacteria; furthermore, TatC homologs have previously been observed to exhibit widely varying expression levels in *E. coli* (Ramasamy et al., 2013), suggesting the importance of sequence-level details in the expression of this IMP.

Wild-type and chimeric TatC expression in *E. coli*

It is first demonstrated that homologs of the IMP TatC exhibit large variance in observed expression levels in *E. coli*. For a quantitative measure of IMP expression, we employ a C-terminal fusion-tag of a green fluorescent protein (GFP) variant (Waldo et al., 1999) (Figure 1A) and measure whole-cell fluorescence by flow cytometry. Whole-cell fluorescence intensity of this fusion-tag has been validated in numerous previous studies to correlate strongly with the amount of folded IMP, rather than the total level of IMP translated (Fluman et al., 2014, Wang et al., 2011, Guglielmi et al., 2011, Geertsma et al., 2008, Drew et al., 2005); we further validate the expression levels measured from whole-cell fluorescence (Figure 1B) using in-gel fluorescence (Figure 1C and Figure S1, Pearson correlation coefficient, $r = 0.914$) and western blot analysis (Figure S1). With this approach, expression levels in *E. coli* are experimentally measured for TatC homologs from a variety of bacteria, including *Aquifex aeolicus* (*Aa*), *Bordetella parapertussis* (*Bp*), *Campylobacter jejuni* (*Cj*), *Deinococcus radiodurans* (*Dr*), *Escherichia coli* (*Ec*), *Hydrogenivirga* sp. 128-5-R1 (*Hy*), *Mycobacterium tuberculosis* (*Mt*), *Staphylococcus aureus* (*Sa*), *Vibrio cholera* (*Vc*), and *Wolinella succinogenes* (*Ws*) (sequences in Figure S2).

Figure 1B demonstrates the wide range of expression levels that are exhibited by the TatC homologs in *E. coli*. Previous expression trials of TatC homologs identified that *Aa*TatC is readily produced at high levels in *E. coli*, which enabled the solution of its structure (Ramasamy et al., 2013, Rollauer et al., 2012). In contrast, low expression is found for both the *Mycobacterium tuberculosis* TatC (hereafter referred to as *Mt*TatC(Wt-tail) and a modified sequence truncating the un-conserved 38-residue sequence of the C-terminal loop (hereafter referred to as *Mt*TatC) (Ramasamy et al., 2013).

To examine the parts of the protein sequence that affect expression, ‘swap chimeras’ were generated by exchanging entire loops and TMDs between *Aa*TatC and *Mt*TatC (sequences in Table S1). The TMDs and loops were defined by comparing sequence alignments and membrane topology predictions (Figure 2B) (Sievers et al., 2011, Tsirigos et al., 2015). The swap chimeras exhibited a wide range of expression results (Figure 2A). The C-terminal loop sequence, referred to as the C-tail and labeled as loop 7 in Figure 1A, was found to have a significant effect on expression levels (shaded bars in Figure 2A). Removal of the *Mt*TatC C-tail improves expression. Removal of the C-tail from the *Aa*TatC sequence leads to a corresponding decrease in expression. Strikingly, swapping the *Aa*TatC C-tail (*Aa*-tail) into the *Mt*TatC sequence leads to a significant improvement in expression.

The positive effect of the *Aa*-tail on *Mt*TatC expression raises the question of whether expression can be similarly improved in other TatC homologs by substituting the corresponding C-tail sequence (Figure 2E) with that of *Aa*TatC. Swapping the C-tail of the various TatC homologs with the *Aa*-tail improved expression in seven out of nine of cases (Figure 2D). Taken together, the results in Figure 2 indicate that the C-tail is a significant factor in determining TatC expression across homologs.

***In silico* modeling of TatC integration**

To investigate the mechanistic basis for the experimentally observed effect of the C-tail on expression, we employ a recently developed *in silico* coarse-grained approach that models cotranslational translocation on unbiased biological timescales (Zhang and Miller, 2012b). The coarse-grained model, which is derived from over 16 μ s of molecular dynamics simulations of the Sec translocation channel, the membrane bilayer, and protein substrates (Zhang and Miller, 2010, Zhang and Miller, 2012a), has been validated for the description of Sec-facilitated membrane integration, including experimentally observed effects of amino-acid sequence on the membrane topology of single-spanning IMPs (Zhang and Miller, 2012b) and multi-spanning dual-topology proteins (Van Lehn et al., 2015). IMP sequences are mapped onto a Brownian dynamics model of the ribosome/translocation-channel/nascent-protein system, and the Sec translocon-facilitated integration of the IMP into the lipid bilayer is directly simulated in 1,200 independent minute-timescale trajectories for each TatC (Figure 3A). The current implementation of the coarse-grained model does not distinguish between expression systems.

Using the results of the coarse-grained model, Figure 3B presents the simulated integration efficiency (*i.e.*, the simulated integration efficiency is defined to be the fraction of trajectories that lead to the correct membrane topology) for several TatC sequences. Unless otherwise specified, we define membrane topology in terms of the final orientation of the C-tail; Figure S3 confirms that analyzing the trajectories in terms of this single-loop definition for membrane topology correlates with defining topology in terms of all loops, while reducing the statistical noise. The *Aa*TatC homolog exhibits significantly higher simulated integration efficiency than the *Mt*TatC homolog, which is consistent with the relative experimental expression levels for the two homologs in Figure 3C. Figure 3B further shows that the *Mt*(*Aa*-tail) chimera recovers the high levels of simulated integration efficiency seen for the *Aa*TatC homolog, further mirroring the experimental trends in IMP expression (Figure 3C). Figure 3D presents an analysis of the orientation of each loop, indicating that only loop 7 is significantly affected swapping the C-tail in the simulations. As is shown schematically in Figure 3E, the simulations find that *Mt*TatC exhibits a large fraction of trajectories in which the C-tail resides in the periplasm, such that the C-terminal TMD (TMD 6) fails to correctly integrate into the membrane.

Additional simulations were performed for the full set of the experimentally characterized TatC homologs (Figure S4), allowing comparison of the computationally predicted shifts in IMP integration with those observed experimentally for IMP expression. For each homolog, Figure 3F compares the effect of swapping the wild-type C-tail with the *Aa*-tail on both the experimental expression level and the simulated integration efficiency. With the exception of *Vc*TatC and *Ec*TatC, Figure 3F shows consistent agreement between the computational and experimental results in *E. coli* upon introducing the *Aa*-tail.

Confirmation of the predicted mechanism

The comparison between simulation and experiment in the previous sections suggests a mechanism in which translocation of the C-tail of TatC into the periplasm leads to a reduction in the observed expression level. To validate this, an experimental *in vivo* assay

based on antibiotic resistance in *E. coli* is employed. The C-terminal GFP tag was replaced by β -lactamase, such that an incorrectly oriented C-tail would confer increased resistance to β -lactam antibiotics (Figure 4A); an inverse correlation between antibiotic resistance and GFP fluorescence is thus expected. *AaTatC*, *Mt*, and *Mt(Aa-tail)* constructs containing the β -lactamase tag were expressed using the same protocol as before. Following expression, the cells were diluted to an OD₆₀₀ of 0.1 in fresh media without inducing agent and then grown to an OD₆₀₀ of approximately 0.5 at which point ampicillin was added. 1.5 hours after ampicillin treatment, equal amounts of the media were plated on LB agar plates without ampicillin (Figure 4B). The number of observed colonies is used to quantify the relative cell survival (Figure 4C, bottom). The survival rate of *Mt(Aa-tail)*, *Mt*, and *AaTatC* inversely correlates with the simulated integration efficiency of the C-tail (Figure 4C), validating the proposed mechanism.

Tail-charge as an expression determinant: Experimental tests of computational predictions

To further establish the connection between the simulated integration efficiencies and the experimentally observed expression levels, we examine the effect of C-tail mutations. We focus on modifications of the C-tail amino-acid sequences that involve the introduction or removal of charged residues, which are known to affect IMP topology and stop-transfer efficiency (Goder and Spiess, 2003, Seppälä et al., 2010, Zhang and Miller, 2012b).

We begin by investigating the generic effect of the C-tail charge magnitude on TatC simulated integration efficiency. Figure 5A presents the results of coarse-grained simulations in which the magnitude of the charges on the C-tail of the *Mt(Aa-tail)* sequence were scaled by a multiplicative factor, χ , keeping all other aspects of the protein sequence unchanged. The simulations reveal that reducing the charge magnitude on the C-tail leads to lower simulated integration efficiency.

To examine the corresponding effect of C-tail charge magnitude on expression levels, Figure 5B plots the ratio of experimentally observed expression for each wild-type homolog relative to its corresponding *Aa-tail* swap chimera versus the total charge magnitude on the wild-type C-tail. Without exception in these data, the expression of wild-type homologs with weakly charged C-tails (relative to the *Aa-tail*) is improved upon swapping with the *Aa-tail*, whereas the expression of homologs with strongly charged C-tails is reduced upon swapping with the *Aa-tail* (*i.e.* all data points in Figure 5B fall into the unshaded quadrants).

Figure 5C further illustrates the effect of charge magnitude on expression by presenting the experimentally observed expression levels for *Aa-tail*(-) swap chimeras, in which the introduced C-tail sequence preserves the charge magnitude of the *Aa-tail* sequence while reversing the net charge (see Figure 2E for the C-tail sequences). Despite the complete reversal of the C-tail charge, the observed correlation between expression and C-tail charge magnitude for these two sets of chimeras is strikingly similar (compare Figures 5B and C).

Finally, we considered a series of mutants of the *Mt(Aa-tail)* chimera, in which the charge magnitude of the *Aa-tail* is reduced by mutating positively charged residues to alanine residues (see Figure 2E for the C-tail sequences). For this series of mutants, Figure 5D (black) shows that the simulated integration efficiency decreases with the charge of the C-

tail, which predicts a corresponding decrease in the experimental expression levels; indeed, the subsequent experimental measurements confirm the predicted trend (Figure 5D, blue). Again using the antibiotic resistance assay to validate the connection between simulated integration efficiency and observed expression, Figure 5E confirms that the simulation results correlate with the relative survival of the *Mt(Aa-tail)* alanine mutants with a β -lactamase tag (Figure 5E, red). In addition to providing evidence for the connection between simulated integration efficiency and observed expression levels, the results in Figure 5 suggest that this link can be used to control IMP expression.

Transferability to another expression system

Beyond the *E. coli* overexpression host, we now examine the transferability of the relation between simulated integration efficiency and experimental expression levels. We employ *Mycobacterium smegmatis*, a genetically tractable model organism that is phylogenetically distinct from *E. coli*. All coding sequences were transferred into an inducible *M. smegmatis* vector, including the linker and C-terminal GFP, and expressed; expression levels were then measured by flow cytometry and validated by western blot.

Figure 6A demonstrates that, as in *E. coli*, the experimentally observed expression levels vary widely among the wild-type TatC homologs in *M. smegmatis*. However, comparison of Figure 6A with Figure 1B reveals that the total expression levels for the homologs in *M. smegmatis* are different from those seen in *E. coli*, although for both systems, the *AaTatC* homolog expresses strongly and *MtTatC* expresses poorly (which is perhaps surprising, given the close evolutionary link between *M. smegmatis* and *M. tuberculosis*). Figure 3F also shows that replacing the wild-type C-tail with the *Aa*-tail in *M. smegmatis* generally increases the experimentally observed expression levels, in general agreement (six out of nine homologs) with the previously discussed simulated integration efficiency results.

Figure 3F further shows that the subset of homologs for which the *Aa*-tail swap chimeras lead to increased levels of expression in *M. smegmatis* is overlapping but different from the subset associated with the *E. coli* results. This emphasizes that although the computed levels of simulated integration efficiency agree with the observed changes in expression levels in both expression systems, the observed expression levels depend upon the expression system, while the simulated integration efficiencies calculated using the current implementation of the coarse-grained model are independent of the expression system. In short, simulated integration efficiency is a predictor of the expression levels in both systems, but it is not the only factor contributing to the observed expression levels.

Continuing with the *M. smegmatis* expression system Figure 6B repeats the comparison between the simulated integration efficiency and the observed expression levels for the series of mutants of the *Mt(Aa-tail)* chimera, in which the positive charge of the *Aa*-tail is reduced by mutating positively charged residues to alanine residues. The simulated integration efficiencies, identical to those in Figure 5D, are predicted to decrease as charges are removed. The experimental expression levels for *M. smegmatis* in Figure 6B likewise show a decrease. Taken together, the results obtained for the *M. smegmatis* expression system suggest that the connection between simulated integration efficiency and observed expression levels may be generalizable beyond *E. coli*.

Transferability beyond the C-tail: Analysis of loop 5 swap chimera

As seen in Figure 3D, the coarse-grained simulations predict poor integration efficiency for loop 5, suggesting an additional location (beyond the C-tail, loop 7) in the *MtTatC* sequence that can be optimized for expression. Figure 7A presents the simulated integration efficiency for loop 5 in each of the TatC homologs, revealing a significant range of efficiencies. Selecting the four homologs with the highest predicted simulated integration efficiency for loop 5 (*Sa*, *Hy*, *Cj*, and *Vc*), chimera proteins were derived from the *MtTatC* sequence by swapping loop 5 of *MtTatC* with the corresponding loop 5 sequence from each of these homologs (Figure 7B). Figure 7C compares the simulated integration efficiency and experimentally observed expression level for each chimera, revealing agreement for three out of four cases. Comparing the simulation results in Figure 7, note that the degree of improvement for the simulated integration efficiency obtained from the coarse-grained simulations of the chimeras (Figure 7C) is different from that anticipated by naïve comparison of the individual loops in the wild-type sequences (Figure 7A); this emphasizes that the simulated integration efficiency is sensitive to elements of the IMP sequence beyond the local segment that is being swapped. The results in Figure 7 suggest the simulated integration efficiency can be used to identify regions beyond the TatC C-tail for modification to improve experimental expression; more generally, it suggests the potential for identifying local segments of an IMP amino-acid sequence that may be modified to yield increased experimental expression.

Discussion

The mechanistic picture that emerges from the experimental and theoretical analysis of the TatC IMP family is that the efficiency of Sec-facilitated membrane integration, which is impacted by the IMP amino-acid sequence, is a key determinant in the degree of observed protein expression. We observed that TatC homologs had varying levels of expression (Figures 1B and 6A). Swap chimeras between *AaTatC* and *MtTatC* revealed a significant effect of the C-tail in determining expression yields (Figure 2A), with the *Aa*-tail having a largely positive effect that was transferrable to other homologs (Figure 3F). Coarse-grained modeling predicted a large, sequence-dependent variation of the simulated integration efficiency for the C-tail (Figure 3), suggesting the underlying mechanism by which the *Aa*-tail enhances the expression of other TatC homologs. Validation of this mechanism was experimentally demonstrated using an antibiotic-resistance assay (Figure 4). Additional point-charge mutations in the C-tail were shown to change the simulated integration efficiency, which in turn predicted changes in the IMP expression levels according to the proposed mechanism; these predictions were experimentally confirmed in both *E. coli* (Figure 5) and *M. smegmatis* (Figure 6). Finally, the link between simulated integration efficiency and experimental expression was exploited to design *MtTatC* chimeras with improved expression based on the loop 5 simulated integration efficiency (Figure 7).

The observed correlation between IMP integration efficiency and observed expression levels presented here is consistent with earlier observations that expression can be modulated by mutations of the sequence (Sarkar et al., 2008, Grisshammer et al., 1993, Warne et al., 2008), as well as recent work in which mis-integrated dual-topology IMPs are shown to be

degraded by FtsH (Woodall et al., 2015). However, these earlier studies did not provide a clear mechanistic basis for the relation between IMP sequence modifications and observed expression levels. In the current work, we demonstrate the relation between integration efficiency and observed expression levels, and we demonstrate a tractable coarse-grained approach for computing the simulated integration efficiency and its changes upon sequence modifications. This work also raises the possibility of using simulated integration efficiencies to optimize experimental expression levels, which has been demonstrated here via the computational prediction and subsequent experimental validation of individual charge mutations in the C-tail and of loop-5 swap chimeras.

A few comments are worthwhile with regard to the scope of the conclusions drawn here. Firstly, the current work focused on comparing protein expression levels among IMP sequences that involve relatively localized changes, such as single mutations or loop swap chimeras, as opposed to predicting relative expression levels among dramatically different IMP sequences. Secondly, the current work examines experimental conditions for the overexpression of IMPs using the same plasmids, which may be expected to isolate the role of membrane integration in determining the relative expression levels of closely related IMP sequences. The prediction of expression levels among IMPs that involve more dramatic differences in sequence may well require the consideration of other factors, beyond just the simulated integration efficiency. Moving forward, we expect that a useful strategy will be to systematically combine the simulated IMP integration efficiency with other sequence-based properties to predict IMP expression levels (Daley et al., 2005).

The experimental and computational tools used here are readily applicable to many systems, potentially aiding the understanding and enhancement of IMP expression in many other systems, as well as providing fundamental tools for the investigation of co-translational IMP folding. By demonstrating inexpensive *in silico* methods for predicting protein expression, we note the potential for computationally guided protein expression strategies to significantly impact the isolation and characterization of many IMPs.

Experimental Procedures

Cloning, expression and flow cytometry

Briefly, for *E. coli* all expression plasmids were derived from pET28(a+)-GFP-ccdB, with the final expressed sequences containing a Met-Gly N-terminus followed by the IMP sequence, a tobacco etch virus (TEV) protease site, a GFP variant (Waldo et al., 1999), and an eight His tag. For β -lactamase constructs, the GFP sequence was replaced by a β -lactamase sequence. For *M. smegmatis* expression plasmids, the entire coding region of the TatC homologs were sub-cloned and transferred into pMyNT vector (Noens et al., 2011). *E. coli* constructs were grown in BL21 Gold (DE3) cells (Agilent Technologies) at 16°C and induced with 1 mM IPTG at an OD₆₀₀ of 0.3 then analyzed after 16 hours. *M. smegmatis* constructs were grown in mc²155 cells (ATCC) at 37°C and induced at an OD₆₀₀ of 0.5 with 0.2% acetamide then analyzed after six hours. A 200 μ L sample of each expression culture was pelleted and resuspended in 1 mL of PBS. Whole-cell GFP fluorescence was measured using a MACSQuant10 Analyzer (Miltenyi). For the ampicillin survival assay, the cells were diluted to an OD₆₀₀ of 0.1 in fresh media following expression without inducing agent and

then grown to an OD₆₀₀ of approximately 0.5 at which point ampicillin was added. 1.5 hours after ampicillin treatment, equal amounts of the media were plated on LB agar plates without ampicillin. The number of observed colonies is used to quantify the relative cell survival. Full experimental protocols are provided in the Supplemental Experimental Procedures.

Description of the CG model

Modeling of IMP integration in the current study was performed using a previously developed coarse-grained (CG) method for the direct simulation of co-translational protein translocation and membrane integration (Zhang and Miller, 2012b). Ribosomal translation and membrane integration of nascent proteins are thus simulated on the minute timescale, enabling direct comparison between theory and experiment. The CG model was previously parameterized using extensive molecular dynamics simulations of the translocon and nascent protein in explicit lipid and water environment (Zhang and Miller, 2012a, Zhang and Miller, 2010). The CG model has been validated against available experimental data and shown to correctly capture effects related to nascent protein charge, hydrophobicity, length, and translation rate in both IMP integration and protein translocation studies (Zhang and Miller, 2012b, Van Lehn et al., 2015). Details of the implementation of the CG model and the analysis of the simulated trajectories are given in the Supplemental Experimental Procedures and Table S2.

Supplementary Material

Refer to Web version on PubMed Central for supplementary material.

Acknowledgements

The authors thank R.C. Van Lehn and D.C. Rees for comments on the manuscript and D. Daley for helpful discussion of (Daley et al., 2005). Work in the Clemons lab is supported by an NIH Pioneer Award to WMC (5DP1GM105385) and an NIH training grant to SSM (NIH/NRSA training grant 5T32GM07616). Work in the Miller group is supported in part by the Office of Naval Research (N00014-10-1-0884) and computational resources were provided by the National Energy Research Scientific Computing Center (NERSC) and a DOE Office of Science User Facility (DE-AC02-05CH11231).

References

- BOGSCH EG, SARGENT F, STANLEY NR, BERKS BC, ROBINSON C, PALMER T. An essential component of a novel bacterial protein export system with homologues in plastids and mitochondria. *J Biol Chem.* 1998; 273:18003–6. [PubMed: 9660752]
- DALEY DO, RAPP M, GRANSETH E, MELÉN K, DREW D, HEIJNE GV. Global Topology Analysis of the Escherichia coli Inner Membrane Proteome. *Science.* 2005; 308:1321–1323. [PubMed: 15919996]
- DREW D, SLOTBOOM DJ, FRISO G, REDA T, GENEVAUX P, RAPP M, MEINDL-BEINKER NM, LAMBERT W, LERCH M, DALEY DO, VAN WIJK KJ, HIRST J, KUNJI E, DE GIER JW. A scalable, GFP-based pipeline for membrane protein overexpression screening and purification. *Protein Sci.* 2005; 14:2011–7. [PubMed: 15987891]
- FLUMAN N, NAVON S, BIBI E, PILPEL Y. mRNA-programmed translation pauses in the targeting of E. coli membrane proteins. *Elife.* 2014; 3

- GEERTSMA ER, GROENEVELD M, SLOTBOOM DJ, POOLMAN B. Quality control of overexpressed membrane proteins. *Proc Natl Acad Sci U S A*. 2008; 105:5722–7. [PubMed: 18391190]
- GODER V, SPIESS M. Molecular mechanism of signal sequence orientation in the endoplasmic reticulum. *EMBO J*. 2003; 22:3645–53. [PubMed: 12853479]
- GRISSHAMMER R, DUCKWORTH R, HENDERSON R. Expression of a rat neurotensin receptor in *Escherichia coli*. *Biochem J*. 1993; 295:571–6. Pt 2. [PubMed: 8240259]
- GUGLIELMI L, DENIS V, VEZZIO-VIE N, BEC N, DARIAVACH P, LARROQUE C, MARTINEAU P. Selection for intrabody solubility in mammalian cells using GFP fusions. *Protein Eng Des Sel*. 2011; 24:873–81. [PubMed: 21997307]
- HARLEY CA, HOLT JA, TURNER R, TIPPER DJ. Transmembrane protein insertion orientation in yeast depends on the charge difference across transmembrane segments, their total hydrophobicity, and its distribution. *J Biol Chem*. 1998; 273:24963–71. [PubMed: 9733804]
- HESSA T, KIM H, BIHLMAIER K, LUNDIN C, BOEKEL J, ANDERSSON H, NILSSON I, WHITE SH, VON HEIJNE G. Recognition of transmembrane helices by the endoplasmic reticulum translocon. *Nature*. 2005; 433:377–381. [PubMed: 15674282]
- LEWINSON O, LEE AT, REES DC. The funnel approach to the precrystallization production of membrane proteins. *J Mol Biol*. 2008; 377:62–73. [PubMed: 18241890]
- NOENS EE, WILLIAMS C, ANANDHAKRISHNAN M, POULSEN C, EHEBAUER MT, WILMANN M. Improved mycobacterial protein production using a *Mycobacterium smegmatis* groEL1DeltaC expression strain. *BMC Biotechnol*. 2011; 11:27. [PubMed: 21439037]
- RAMASAMY S, ABROL R, SULOWAY CJ, CLEMONS WM JR. The glove-like structure of the conserved membrane protein TatC provides insight into signal sequence recognition in twin-arginine translocation. *Structure*. 2013; 21:777–88. [PubMed: 23583035]
- RAPOPORT TA. Protein translocation across the eukaryotic endoplasmic reticulum and bacterial plasma membranes. *Nature*. 2007; 450:663–9. [PubMed: 18046402]
- ROLLAUER SE, TARRY MJ, GRAHAM JE, JAASKELAINEN M, JAGER F, JOHNSON S, KREHENBRINK M, LIU SM, LUKEY MJ, MARCOUX J, MCDOWELL MA, RODRIGUEZ F, ROVERSI P, STANSFELD PJ, ROBINSON CV, SANSOM MS, PALMER T, HOGBOM M, BERKS BC, LEA SM. Structure of the TatC core of the twin-arginine protein transport system. *Nature*. 2012; 492:210–4. [PubMed: 23201679]
- SARKAR CA, DODEVSKI I, KENIG M, DUDLI S, MOHR A, HERMANS E, PLUCKTHUN A. Directed evolution of a G protein-coupled receptor for expression, stability, and binding selectivity. *Proc Natl Acad Sci U S A*. 2008; 105:14808–13. [PubMed: 18812512]
- SCHLEGEL S, KLEPSCH M, GIALAMA D, WICKSTROM D, SLOTBOOM DJ, DE GIER JW. Revolutionizing membrane protein overexpression in bacteria. *Microb Biotechnol*. 2010; 3:403–11. [PubMed: 21255339]
- SCOTT DJ, KUMMER L, TREMMEL D, PLUCKTHUN A. Stabilizing membrane proteins through protein engineering. *Curr Opin Chem Biol*. 2013; 17:427–35. [PubMed: 23639904]
- SEPPÄLÄ S, SLUSKY JS, LLORIS-GARCERÁ P, RAPP M, VON HEIJNE G. Control of Membrane Protein Topology by a Single C-Terminal Residue. *Science*. 2010
- SIEVERS F, WILM A, DINEEN D, GIBSON TJ, KARPLUS K, LI W, LOPEZ R, MCWILLIAM H, REMMERT M, SODING J, THOMPSON JD, HIGGINS DG. Fast, scalable generation of high-quality protein multiple sequence alignments using Clustal Omega. *Mol Syst Biol*. 2011; 7:539. [PubMed: 21988835]
- TSIRIGOS KD, PETERS C, SHU N, KALL L, ELOFSSON A. The TOPCONS web server for consensus prediction of membrane protein topology and signal peptides. *Nucleic Acids Res*. 2015; 43:W401–7. [PubMed: 25969446]
- VAN LEHN RC, ZHANG B, MILLER TF. Regulation of multispinning membrane protein topology via post-translational annealing. *Elife*. 2015; 4
- VON HEIJNE G. The distribution of positively charged residues in bacterial inner membrane proteins correlates with the trans-membrane topology. *EMBO J*. 1986; 5:3021–7. [PubMed: 16453726]
- WAGNER S, BADER ML, DREW D, DE GIER JW. Rationalizing membrane protein overexpression. *Trends Biotechnol*. 2006; 24:364–71. [PubMed: 16820235]

- WALDO GS, STANDISH BM, BERENDZEN J, TERWILLIGER TC. Rapid protein-folding assay using green fluorescent protein. *Nat Biotechnol.* 1999; 17:691–5. [PubMed: 10404163]
- WANG Z, XIANG Q, WANG G, WANG H, ZHANG Y. Optimizing expression and purification of an ATP-binding gene *gsiA* from *Escherichia coli* k-12 by using GFP fusion. *Genet Mol Biol.* 2011; 34:661–8. [PubMed: 22215971]
- WARNE T, SERRANO-VEGA MJ, BAKER JG, MOUKHAMETZIANOV R, EDWARDS PC, HENDERSON R, LESLIE AGW, TATE CG, SCHERTLER GFX. Structure of a beta(1)-adrenergic G-protein-coupled receptor. *Nature.* 2008; 454:486–U2. [PubMed: 18594507]
- WOODALL NB, YIN Y, BOWIE JU. Dual-topology insertion of a dual-topology membrane protein. *Nat Commun.* 2015; 6:8099. [PubMed: 26306475]
- ZHANG B, MILLER TF 3RD. Hydrophobically stabilized open state for the lateral gate of the Sec translocon. *Proc Natl Acad Sci U S A.* 2010; 107:5399–404. [PubMed: 20203009]
- ZHANG B, MILLER TF 3RD. Direct simulation of early-stage Sec-facilitated protein translocation. *J Am Chem Soc.* 2012a; 134:13700–7. [PubMed: 22852862]
- ZHANG B, MILLER TF 3RD. Long-timescale dynamics and regulation of Sec-facilitated protein translocation. *Cell Rep.* 2012b; 2:927–37. [PubMed: 23084746]

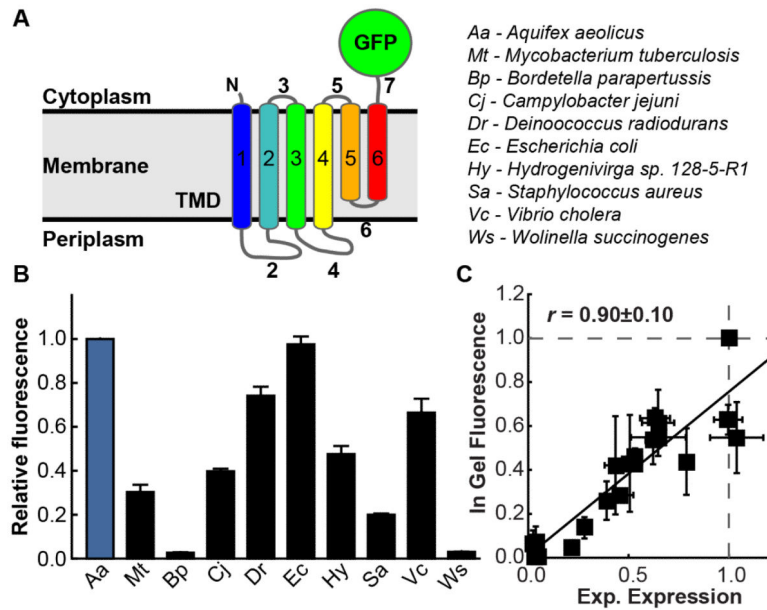


Figure 1. Variation in the expression of TatC homologs in *E. coli*.

(A) A topology representation of TatC with a GFP C-terminal tag, as used in the expression studies. TMDs and loops are indicated in colors and gray, respectively, and are numbered.

(B) Expression levels of various TatC homologs in *E. coli*, measured by TatC-GFP fluorescence, with expression levels normalized to *Aa*TatC (blue). Error bars indicate the standard error of mean.

(C) Correlation of the in-gel fluorescence quantified for each band versus the experimental expression measured by flow cytometry. Both metrics are highly correlated across multiple trials (Pearson correlation coefficient $R = 0.90 \pm 0.10$) with in-gel fluorescence showing the same trends in expression yield as seen by flow-cytometry. Error bars indicate the standard error of mean. See also Figure S1.

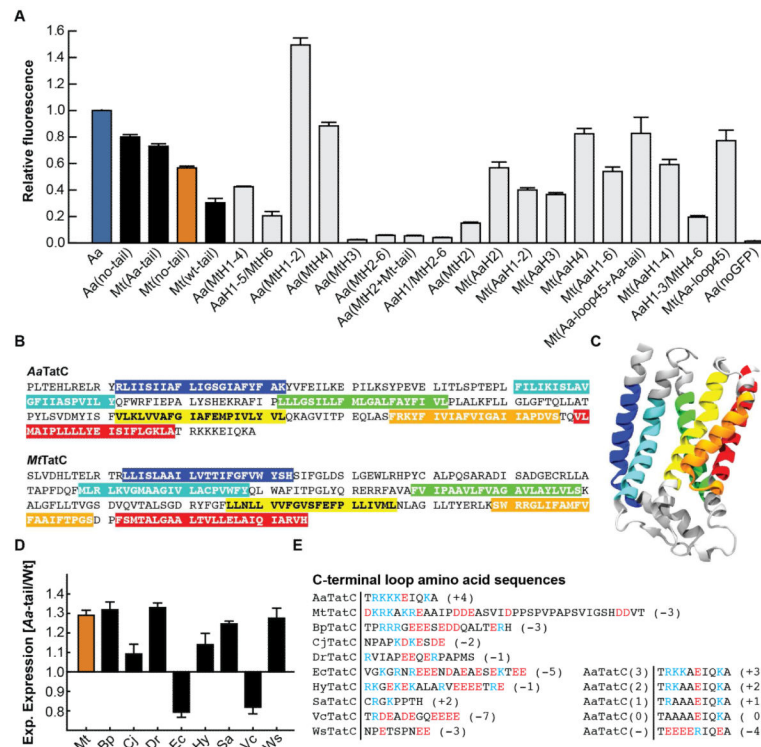


Figure 2. Effect of the C-tail on TatC expression in *E. coli*.

(A) Measured expression levels of the *AaTatC* and *MtTatC* chimera proteins, normalized to *AaTatC*. Shaded bars represent wild-type TatC homologs and mutants with C-tail modifications. (B) Domain definitions used in generating the swap chimeras, with TMDs highlighted. (C) A ribbons diagram of the structure of *AaTatC* (pdbID 4HTS). TMDs are colored according to the highlights used in part (B). (D) For each homolog, the ratio of the measured expression level for the *Aa*-tail chimera to that of the corresponding wild-type sequence. (E) TatC wild-type and charge mutant C-tail sequences. Positive residues are in blue and negative residues are in red. The net charge is shown to the right of each sequence. Error bars indicate the standard error of mean.

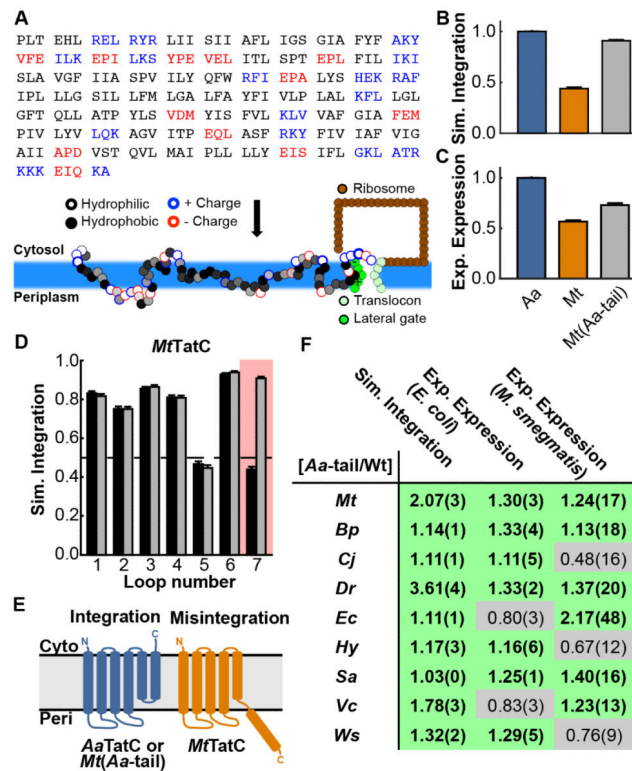


Figure 3. Calculation of TatC integration efficiencies

(A) Schematic illustration of the CG simulation model that is used to model co-translational IMP membrane integration. The amino-acid sequence of the IMP is mapped onto CG beads, with each consecutive trio of amino-acid residues in the nascent protein sequence mapped to an associated CG bead; the underlying properties of the amino-acid residues determine the interactions of the CG beads, as described in the text. (B) Simulated integration efficiency of the *AaTatC*, *MtTatC*, and *Mt(Aa-tail)* sequences. (C) Experimental expression of the *AaTatC*, *MtTatC*, and *Mt(Aa-tail)* sequences. (D) The simulated integration efficiency for individual loops of both the wild-type *MtTatC* sequence (black bars) and the *Aa-tail* swap chimera (grey bars), with loop 7 highlighted. (E) Schematic of the correct and incorrect TatC topologies observed in the simulations; misintegration of loop 7 and translocation of TMD 6 leads to an incorrect final topology for *MtTatC*. Error bars indicate the standard error of mean. (F) For each homolog, comparison between the experimental expression levels in *E. coli* and *M. smegmatis* and the simulated integration efficiencies, reporting the ratio of the *Aa-tail* chimera result to that of the corresponding wild-type sequence. Ratios exceeding unity are highlighted in green, indicating enhancement due to the *Aa-tail*. Values in parentheses indicate the standard error of mean. See also Figure S4.

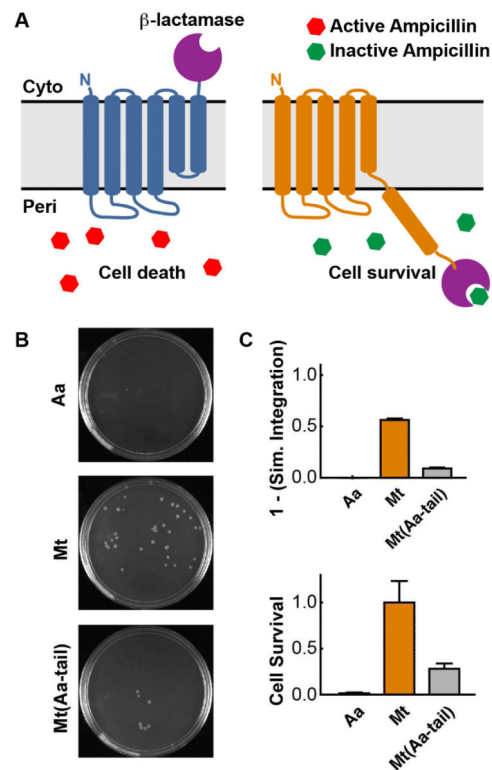


Figure 4. Correlation of antibiotic resistance to membrane topology

(A) Schematic of the cytoplasmic and periplasmic topologies of the TatC C-tail with the fused β -lactamase enzyme. Misintegration of loop 7 leads to periplasmic localization of the β -lactamase, resulting in enhanced antibiotic resistance and cell survival. (B) Representative plates from the ampicillin survival test. (C) Comparison of the simulated integration efficiency (top) and relative ampicillin survival rate (bottom) for *Aa*TatC, *Mt*TatC, and *Mt(Aa-tail)*. The reported cell survival corresponds to the ratio of counted cells post-treatment versus prior to treatment with ampicillin; all values are reported relative to *Mt*TatC. Error bars indicate the standard error of mean.

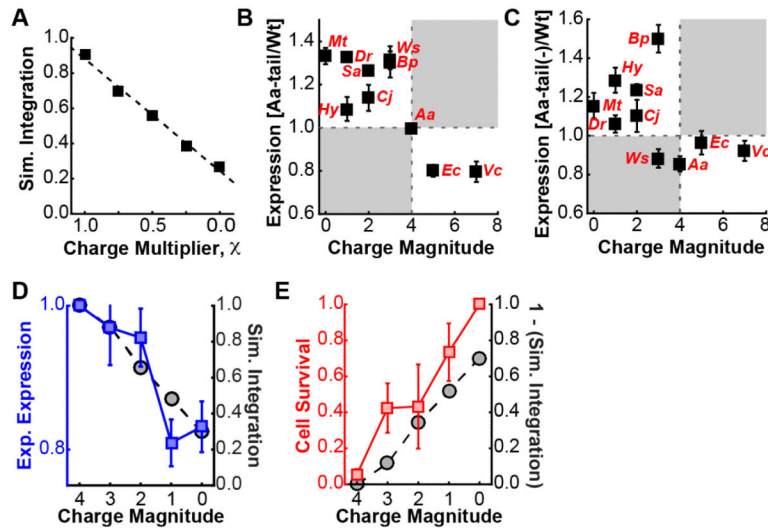


Figure 5. Mechanistic basis associated with charged C-tail residues

(A) Simulated integration efficiency of the *Mt(Aa-tail)* chimera, as a function of scaling the charges of the C-tail residues. (B) Correlation of the ratio of the measured expression for the *Aa-tail* swap chimeras to that of the corresponding wild-type sequence versus the charge magnitude of the wild-type C-tail (data from Figure 2B and Figure 2E). Linear regression yields a fit of $R = -0.8 \pm 0.2$. (C) Correlation of the ratio of the measured expression for the *Aa-tail(-)* swap chimeras to that of the corresponding wild-type sequence versus the charge magnitude of the wild-type C-tail, where the *Aa-tail(-)* swap chimeras include a variant of the *Aa-tail* with net negative charge and the same overall charge magnitude. (D) Experimental expression levels in *E. coli* (blue, left axis) and simulated integration efficiency (black, right axis) for a series of mutants of the *Mt(Aa-tail)* sequence, in which positively charged residues in the *Aa-tail* are mutated to alanine residues. Reported values are normalized to *Mt(Aa-tail)*. (E) Relative ampicillin survival rate in *E. coli* (red, left axis) and simulated integration efficiency (black, right axis) for a series of mutants of the *Mt(Aa-tail)* sequence, in which positively charged residues in the *Aa-tail* are mutated to alanine residues. Simulation results are normalized as in part (d), while ampicillin survival is normalized to the highest survival rate (*i.e.*, with zero charge magnitude). Error bars indicate the standard error of mean.

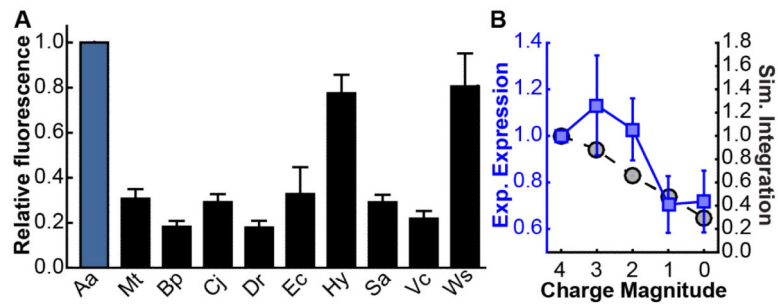


Figure 6. *M. smegmatis* expression tests

(A) Expression levels of various TatC homologs in *M. smegmatis*, measured by TatC-GFP fluorescence, with expression levels normalized to *Aa*TatC (blue). (B) Simulated integration efficiency (blue, left axis) and measured expression levels in *M. smegmatis* (black, right axis) for a series of mutants of the *Mt*(*Aa*-tail) sequence, in which positively charged residues in the *Aa*-tail are mutated to alanine residues. Error bars indicate the standard error of mean.

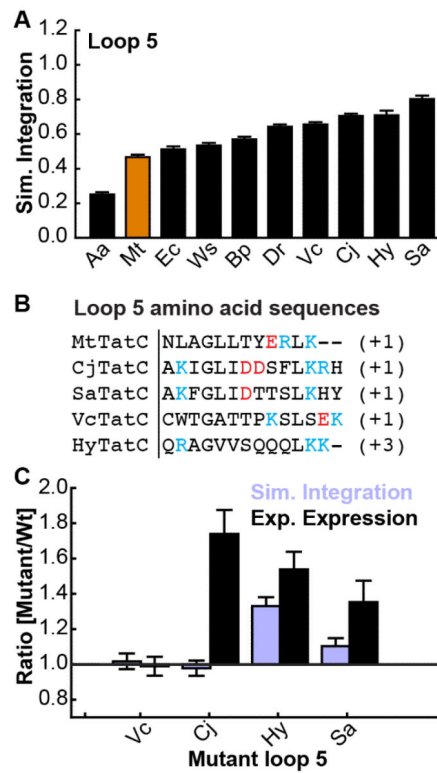


Figure 7. Loop 5 analysis for *MtTatC*

(A) Simulated integration efficiency of loop 5 for the TatC homologs. (B) Loop 5 amino-acid sequence for various TatC homologs. (C) Experimental expression (black) and simulated integration efficiency (purple) for the loop 5 swap chimeras of *MtTatC* in which the entire loop 5 sequence of wild-type *MtTatC* is replaced with the corresponding sequence of other homologs. Error bars indicate the standard error of mean.